Activation of CH 4 by Gas-Phase Mo + , and the Thermochemistry of Mo−ligand Complexes †

ARTICLE *in* THE JOURNAL OF PHYSICAL CHEMISTRY A · AUGUST 2006

Impact Factor: 2.69 · DOI: 10.1021/jp056804o · Source: PubMed

1 AUTHOR:

P. B. Armentrout
University of Utah
492 PUBLICATIONS **20,541** CITATIONS

SEE PROFILE

Activation of CH_4 by Gas-Phase Mo^+, and the Thermochemistry of Mo−ligand Complexes†

P. B. Armentrout

Department of Chemistry, University of Utah, Salt Lake City, Utah 84112

Received: November 23, 2005; In Final Form: January 26, 2006

The kinetic-energy dependence of the reactions of Mo^+ (^6S) with methane has been studied using guided ion beam mass spectrometry. No exothermic reactions are observed in this system, as also found previously, but efficient dehydrogenation occurs at slightly elevated energies. At higher energies, MoH^+ dominates the product spectrum and MoC^+, $MoCH^+$, and $MoCH_3^+$ are also observed. Modeling of the endothermic reaction cross sections yields the 0 K bond dissociation energies (in eV) of $D_0(Mo^+-C) = 4.55 \pm 0.19$, $D_0(Mo^+-CH) = 5.32 \pm 0.14$, $D_0(Mo^+-CH_2) = 3.57 \pm 0.10$, and $D_0(Mo^+-CH_3) = 1.57 \pm 0.09$. The results for Mo^+ are compared with those for the first- and third-row transition-metal congeners, Cr^+ and W^+, and the differences in behavior and mechanism are discussed. Theoretical results are used to elucidate the geometric and electronic structures of all product ions as well as the complete potential-energy surface for reaction. The efficiency of the coupling between the sextet and quartet spin surfaces is also quantified.

1. Introduction

A long-term goal of research in our laboratory has been the study of the reactions of transition-metal ions (M^+) with small hydrocarbons. Such studies can reveal the electronic requirements for the activation of C−H and C−C bonds at metal centers[1−4] and provide an examination of the periodic trends in such reactivity unavailable in condensed-phase media.[1,5] A particular strength of the guided ion beam methods used in our laboratory is the derivation of metal−hydrogen and metal−carbon bond dissociation energies (BDEs).[6−9] Such thermochemistry is of obvious fundamental interest and also has implications in understanding a variety of catalytic reactions involving transition-metal systems.[10] Studies of such systems for first-row transition-metal elements is extensive,[1−8] whereas studies of the reactivity of second-row transition-metal cations[11−14] are somewhat less systematic.[9] In our laboratory, we have studied the activation of methane by most of the second-row transition-metal ions: Y^+,[15] Zr^+,[16] Nb^+,[17] Rh^+,[18] Pd^+,[19] and Ag^+.[20]

In the present study, we progress toward completion of the second-row series by examining Mo^+ and describe its reactions with methane. This system has been studied previously by Schilling and Beauchamp,[11] who used an ion beam apparatus to examine this system at low kinetic energies, and then by Cassady and McElvany,[14] who used ion cyclotron resonance (ICR) mass spectrometry to study the system at thermal energies. In neither case were any reactions observed. Here, we probe the reactions of Mo^+ with the simplest saturated hydrocarbon more quantitatively by investigating over a wide range of kinetic energies. This permits the extraction of systematic thermodynamic as well as mechanistic information.

There is relatively little thermochemistry available for gas-phase molybdenum species in the literature.[8] We previously measured BDEs for Mo^+-H, Mo^+-C, and Mo^+-O by determining the endothermicities of the formation of these species from reactions of Mo^+ with H_2 (and D_2)[21] and CO.[22] Sallans et al. measured the neutral Mo−H bond energy by bracketing the proton affinity of Mo^-.[23] In addition, theoretical calculations have been performed for the BDEs of several species relevant to the present work: MoH^+,[24−27] $MoCH_2^+$,[28] and $MoCH_3^+$.[29,30] Theoretical studies of MoC^+ have not been performed, and no experimental thermochemistry is available in the literature for $MoCH^+$, $MoCH_2^+$, or $MoCH_3^+$. In the present work, we measure BDEs for all four $MoCH_x^+$ species by determining the endothermic reaction thresholds for reactions of Mo^+ with methane. We also perform theoretical calculations at several levels for all of these species.

One of the challenging problems in the study of alkane activation by transition-metal ions is to determine reaction mechanisms. Detailed experimental[31−35] and theoretical[36−40] studies of first-row transition-metal cations (mostly Fe^+, Co^+, and Ni^+) have been carried out to elucidate the mechanisms, whereas fewer studies that emphasize mechanisms for second-row transition-metal cations have been performed.[12,18,36] Nevertheless, it is clear that the mechanisms do vary, both from early to late and from first-row to second-row transition-metal cations, as reviewed[9] elsewhere. Here, we examine the mechanisms for reactions of Mo^+ both experimentally and computationally and compare them to those for the first- and third-row congeners, Cr^+ and W^+.[41−44]

2. Experimental and Theoretical Section

2.1. General. These studies are performed using a guided ion beam tandem mass spectrometer. The instrumental and experimental methods have been described previously.[45,46] Ions, formed as described below, are extracted from the source, accelerated, and focused into a magnetic sector momentum analyzer for mass analysis. The ions are decelerated to a desired kinetic energy and focused into an octopole ion guide that radially traps the ions. While in the octopole, the ions pass through a gas cell that contains the neutral reactant at pressures where multiple collisions are improbable (<0.30 mTorr). Single-collision conditions were verified by examining the pressure dependence of the cross sections measured here. The product ions and reactant ion beam drift out of the gas cell, are focused into a quadrupole mass filter, and are then detected by a

† Part of the "Chava Lifshitz Memorial Issue".

10.1021/jp056804o CCC: $33.50
Published on Web 02/28/2006

secondary electron scintillation detector. Ion intensities are converted to absolute cross sections as described previously.[45] Uncertainties in the absolute cross sections are estimated at ±20%. In some cases, the product cross sections have been corrected for mass overlap between products ions having adjacent masses. Such corrections are generally unambiguous because the various product ions have distinct energy dependences.

To determine the absolute zero and distribution of the ion kinetic energy, the octopole is used as a retarding energy analyzer.[45] The uncertainty in the absolute energy scale is ±0.05 eV (lab). The full width at half-maximum (fwhm) of the ion energy distribution is 0.2−0.4 eV (lab). Lab energies are converted into center-of-mass energies using $E(\mathrm{CM}) = E(\mathrm{lab})m/(m + M)$, where M and m are the ion and neutral reactant masses, respectively. All energies below are in the center-of-mass frame.

2.2. Ion Source. The ion source used here is a dc discharge/flow tube (DC/FT) source described in previous work.[46] The DC/FT source utilizes a molybdenum cathode held at 1.5−3 kV over which a flow of approximately 90% He and 10% Ar passes at a typical pressure of ~0.5 Torr. Ar^+ ions created in a direct current discharge are accelerated toward the molybdenum cathode, sputtering off atomic metal ions. The ions then undergo ~10^5 collisions with He and ~10^4 collisions with Ar in the meter-long flow tube before entering the guided ion beam apparatus. Results obtained previously[21] indicate that the Mo^+ ions produced in the DC/FT source are exclusively in their a^6S ground state (less than 0.1% excited states).

2.3. Data Analysis. Previous theoretical[47,48] and experimental work[49] has shown that endothermic cross sections can be modeled using eq 1

$$\sigma(E) = \sigma_0 \Sigma g_i (E + E_{\mathrm{el}} + E_i - E_0)^n/E \qquad (1)$$

where σ_0 is an energy-independent scaling parameter, E is the relative translational energy of the reactants, E_{el} is the average electronic energy of the reactants (0 in the present case), E_0 is the reaction threshold at 0 K, and n is a parameter that controls the shape of the cross section. The summation is over each rovibrational state of the reactants having relative populations g_i and energies E_i. The various sets of vibrational frequencies used in this work are taken from the literature.[50]

Before comparison with the data, the model is convoluted over the neutral and ion kinetic-energy distributions using previously developed methods.[45,47] The parameters E_0, σ_0, and n are then optimized using a nonlinear least-squares analysis in order to best reproduce the data. Reported values of E_0, σ_0, and n are mean values for each parameter from the best fits to several independent sets of data, and uncertainties are one standard deviation from the mean. The listed uncertainties in the E_0 values also include the uncertainty in the absolute energy scale.

2.4. Theoretical Approach. Most quantum chemistry calculations here are computed with the B3LYP hybrid density functional method,[51−53] and all are performed with the GAUSSIAN 03 suite of programs.[54] In all cases, the thermochemistry reported here is corrected for zero-point energy (ZPE) effects (with frequencies scaled by 0.989).[55] Because several of the transition states of interest here involve bridging hydrogens, the rather large 6-311++G(3df,3p) basis set is used for carbon and hydrogen. This basis set gives good results for the thermochemistry of methane and dihydrogen, with deviations from experiment of less than 0.08 eV for the bond energies (theory vs experiment) of $H-CH_3$ (4.410 vs 4.480 eV), H_2-CH_2 (4.670 vs 4.713 eV), H−CH (4.334 vs 4.360 eV), C−H (3.534 vs 3.465 eV), and H−H (4.508 vs 4.478 eV). The basis set on molybdenum was the Hay−Wadt (n+1) ECP VDZ (HW),[56] equivalent to the Los Alamos ECP (LANL2DZ) basis set, in which 28 core electrons are described by a relativistic effective core potential (ECP).[57] For reasons described below, additional calculations were performed using the Stuttgart−Dresden (SD) ECP and basis set[58] for the most stable states of the various reactants, products, and intermediates. In a late addition to the paper, we also tested the addition of the f-polarization functions described by Frenking and co-workers for the Hay−Wadt ECP (HW*)[59] for comparison with experimental thermochemistry.

TABLE 1: Calculated Excitation Energies (eV) for Mo^+

	HW		HW*		SD	
	^6D	^4G	^6D	^4G	^6D	^4G
B3LYP	2.255	1.924	2.224	1.909	1.379	1.888
BHLYP	2.310	2.059	2.264	2.024	1.531	2.025
MP2(full)	1.885	2.682	2.126	2.740	1.137	2.879
QCISD(T)	1.881	2.484	2.084	2.517	1.107	2.323
exp	1.587	1.906	1.587	1.906	1.587	1.906

To examine the thermochemistry of the ground states for each of the product species, we also utilized the Becke Half and Half LYP (BHLYP),[60,61] MP2(full),[62] and QCISD(T)[63] approaches in addition to B3LYP. Geometry optimizations were independently conducted at each of these levels of theory except for QCISD(T), where B3LYP geometries were used. MP2(full) geometries were also tested, but in all cases, lower energies were obtained at the QCISD(T)//B3LYP level than for QCISD(T)//MP2. These four theoretical approaches yield widely varying results for calculations of the excited states of Mo^+. Experimental values for the splitting between the $^6S(4d^5)$ ground state and the $^6D(5s^14d^4)$, $^4G(4d^5)$, and $^2D(4d^5)$ excited states (averages of properly weighted spin−orbit components of these terms) are 1.587, 1.906, and 2.804 eV, respectively.[64] Values for the ^6D and ^4G states calculated at several levels of theory using the HW, HW*, and SD basis sets are given in Table 1. (In all cases, it was verified that the calculations were for pure $^6S(4d^5)$, $^6D(5s^14d^5)$, and $^4G(4d^5)$ states with no spin contamination.) The SD values for the ^6D state are systematically lower than the HW values calculated at the same level of theory (by 0.79 ± 0.06 eV), whereas the HW* values are relatively constant and similar to the HW values. The SD basis set appears to handle the d−s excitation energy slightly more accurately than the HW or HW* basis sets for molybdenum when the DFT approaches are used. The ^4G state excitation energies calculated using the HW, HW*, and SD basis sets are fairly close to one another, with the DFT calculations reproducing the experimental value most closely. No single level of theory describes both experimental excitation energies accurately, although the BHLYP/SD approach comes closest.

For many of the species examined here, calculations of excited states were obtained by explicitly moving electrons into other orbitals to create states of alternate configuration and/or symmetry. Optimizations of the geometry were then carried out in the usual way. In all cases, these calculations were conducted at the B3LYP/HW/6-311++G(3df,3p) level.

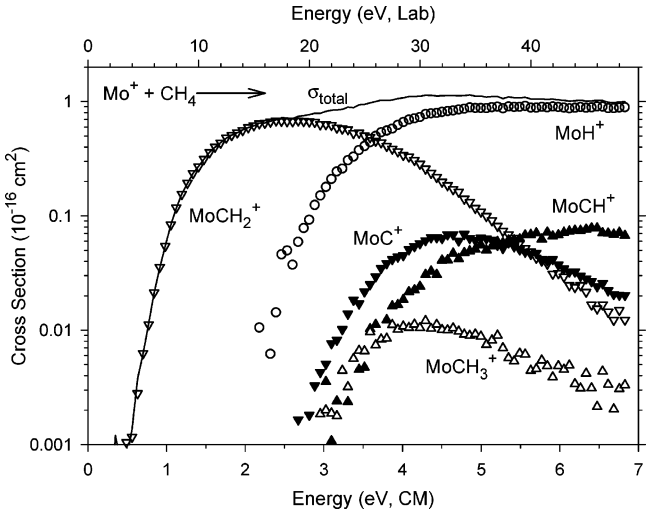

Figure 1. Cross sections for reactions of Mo^+ with CH_4 as a function of kinetic energy in the center-of-mass (lower axis) and laboratory (upper axis) frames.

3. Results

Reaction of Mo^+ with methane yields the products indicated in reactions 2−6 and shown in Figure 1.

$$Mo^+ + CH_4 \rightarrow MoH^+ + CH_3 \quad (2)$$

$$\rightarrow MoC^+ + 2\,H_2 \quad (3)$$

$$\rightarrow MoCH^+ + H_2 + H \quad (4)$$

$$\rightarrow MoCH_2^+ + H_2 \quad (5)$$

$$\rightarrow MoCH_3^+ + H \quad (6)$$

In previous investigations of this reaction at thermal energies and slightly elevated kinetic energies, no reactivity was observed,[11,14] consistent with our failure to observe any reaction below 0.5 eV. The lowest energy pathway observed is dehydrogenation of methane to form $MoCH_2^+$, reaction 5. The cross section rises from an apparent threshold near 0.5 eV and continues to rise until near 2.5 eV, where it starts to decline. $MoCH_2^+$ can decompose by losing CH_2 to form Mo^+ starting at 4.71 eV = $D_0(H_2-CH_2)$[19] by dehydrogenation to form MoC^+ or by losing an H atom to form $MoCH^+$. Clearly the former channel begins too high in energy to account for the decline and neither the $MoCH^+$ or MoC^+ channel has sufficient intensity to account for all of the decline. Instead, we find that the increase in the MoH^+ cross section essentially compensates for the decline observed in the $MoCH_2^+$ cross section, indicating that formation of $MoCH_2^+$ is reduced primarily by depletion of a common intermediate that more easily yields MoH^+ at higher energies, as discussed below.

The MoH^+ cross section rises from an apparent threshold near 2 eV and continues rising until ∼5 eV where it levels off. The other primary product formed in this system is $MoCH_3^+$, formed in reaction 6. The cross section for this product is small, apparently the result of competition with the nearly isoenergetic reaction 2 and rapid dehydrogenation to form $MoCH^+$. This sequence is more evident in the reactions of Mo^+ with the larger alkanes.[65] The $MoCH^+$ and MoC^+ cross sections begin to rise near 3 and 2.7 eV, respectively. The $MoCH^+$ species comes mainly from dehydrogenation of the primary $MoCH_3^+$ product, and the MoC^+ product must result from dehydrogenation of the primary $MoCH_2^+$ product.

4. Thermochemical Results

The energy dependences of the various cross sections are interpreted using eq 1. The optimum values of the parameters of eq 1 are listed in Table 2. The threshold can then be related to thermodynamic information assuming that this represents the energy of the product asymptote, an assumption that is usually correct for ion−molecule reactions because of the long-range attractive forces. Thus, eq 7 is used to derive the BDEs provided in Table 2 where L is the ligand of interest.

$$D_0(Mo^+-L) = D_0(CH_4-L) - E_0 \quad (7)$$

Thermodynamic information for the stable and radical hydrocarbons required to interpret these results has been compiled.[19] Because our bond-energy determination carefully includes all sources of reactant energy, the thermochemistry obtained is for 0 K.

In the following sections our experimental bond energies and theoretical results for each of the product ions observed are compared with experimental and theoretical results from the literature. This thermodynamic information is summarized in Table 3, whereas the theoretical structures found here are provided in Table 4. Additional theoretical results are found in the Supporting Information, which includes the energies and zero-point energies of all reactants and products calculated using several levels of theory (Table S1) as well as energies and zero-point energies (Table S2) and geometries (Table S3) of excited-state species calculated at the B3LYP/HW level.

4.1. MoH^+. A reliable value for $D_0(Mo^+-H)$, Table 3, has previously been determined from the reactions of Mo^+ with H_2 and D_2.[21] The value of 1.72 ± 0.06 eV is in good agreement with high-level theoretical calculations,[24−27] in particular those from Petersson et al.[25] and Das and Balasubramanian.[26] Using this BDE, the predicted threshold for reaction 2 is 2.76 ± 0.06 eV. The threshold measured for this process, Table 2, is slightly higher, by about 0.2 eV, just outside the combined uncertainties. Such a shift can be attributed to competition with the more favorable dehydrogenation process.

Our own calculations find a ground state for MoH^+ of $^5\Sigma^+$, as also found previously.[24−27] This species has a valence electron configuration of $\sigma_b^2\pi^2\delta^2$ in which the bonding orbital is σ_b (73% 4d and 20% 5s character according to Schilling et al.[24]) and the π and δ orbitals are molybdenum-based 4d orbitals. As found by Holthausen et al.[60] for the first-row transition-metal methyl cations, the B3LYP functional tends to overbind singly bound species, giving bond energies of 1.89, 1.92, and 2.02 eV for the HW, HW*, and SD basis on Mo, respectively. In contrast, the BHLYP functional gives better agreement with experiment, 1.60, 1.63, and 1.74 eV, respectively, as does the QCISD(T) approach, 1.65, 1.62, and 1.78 eV, respectively, results that parallel the findings of Holthausen et al. The MP2 method yields bond energies that are somewhat weak, 1.30, 1.30, and 1.47 eV, respectively. Note that the SD basis gives bond energies systematically higher than the HW or HW* basis, by averages of 0.14 ± 0.04 eV, and the best agreement with experiment is found for the SD approach. These trends continue for all species examined here.

We also located several excited states of MoH^+ (Tables S2 and S3). $^5\Pi$ ($\sigma_b^2\pi^1\delta^2\sigma^1$) and $^5\Delta$ ($\sigma_b^2\pi^2\delta^1\sigma^1$) states are found 1.14 and 1.21 eV above the ground state, where the additional σ orbital is largely Mo(5s). Schilling et al.[24] also found these

TABLE 2: Optimized Parameters of Eq 1 for $Mo^+ + CH_4$ System

reactants	products	σ_0, 10^{-16} cm^2 eV^{1-n}	n	E_0, eV	$D_0(Mo^+\text{-L})$, eV
$Mo^+ + CH_4$	$MoH^+ + CH_3$	2.20 (0.33)	0.9 (0.1)	2.95 (0.05)	1.53 (0.05)
	$MoC^+ + 2H_2$	0.21 (0.05)	0.8 (0.3)	3.44 (0.11)	4.62 (0.11)
	$MoCH^+ + H_2 + H$	0.18 (0.04)	0.8 (0.3)	3.95 (0.30)	5.12 (0.30)
	$MoCH_2^+ + H_2$	1.18 (0.55)	1.1 (0.1)	1.14 (0.10)	3.57 (0.10)
	$MoCH_3^+ + H$	0.035 (0.018)	1.1 (0.3)	3.04 (0.11)	1.44 (0.11)

TABLE 3: Experimental and Theoretical Mo^+-L Bond Energies (eV) at 0 K

	this work[a]														
		B3LYP			BHLYP			MP2 (full)			QCISD(T)			previous work	
species	exp	HW	HW*	SD	HW	HW*	SD	HW	HW*	SD	HW	HW*	SD	exp	theory
Mo^+-H		1.892	1.917	2.025	1.599	1.632	1.738	1.295	1.301	1.468	1.651	1.622	1.781	1.72 (0.06)[b]	1.35,[c] 1.53 (0.13),[d] 1.79,[e] 1.91[f]
Mo^+-C	4.55 (0.19)	3.960	4.123	4.162	2.653	2.875	2.870	4.114	4.309	4.387	4.167	4.273	4.339	4.31 (0.20)[g]	
Mo^+-CH	5.32 (0.14)	4.738	4.834	4.918	3.638	3.743	3.831	4.032	4.263	4.175	4.842	4.916	4.909		
Mo^+-CH_2	3.57 (0.10)	3.279	3.346	3.440	2.551	2.617	2.717	2.580	2.725	2.729	2.956	3.222	3.271		3.08 (0.17)[h]
Mo^+-CH_3	1.57 (0.09)	1.756	1.800	1.889	1.323	1.371	1.458	1.493	1.635	1.647	1.705	1.742	1.804		1.38 (0.13),[i] 1.31[j]
MAD[k]		0.38	0.31	0.32	0.98	0.90	0.82	0.63	0.53	0.51	0.35	0.26	0.26		

[a] Theoretical values at the B3LYP, BHLYP, MP2(full), and QCISD(T)//B3LYP levels using either the Hay−Wadt (HW), Hay−Wadt with f polarization (HW*), or Stuttgart−Dresden (SD) basis set on Mo and 6-311++G(3df,3p) basis on C and H. Experimental values come from Table 2 except as noted in the text. [b] Reference 21. [c] Reference 24. [d] Best estimate value including corrections for errors in the computed atomic splittings (0.09 eV) and basis set incompleteness (0.04 eV) from ref 25. [e] Reference 26. [f] Reference 27. [g] Reference 22. [h] Reference 28. [i] Reference 29. [j] Reference 30. [k] Mean absolute deviation from experimental values.

TABLE 4: MoL^+ Bond Lengths (Å) and Bond Angles (deg) Calculated at Several Levels of Theory

		B3LYP		BHLYP		MP2(full)	
species		HW	SD	HW	SD	HW	SD
MoH^+ ($^5\Sigma^+$)	r(Mo−H)	1.673	1.676	1.670	1.672	1.637	1.645
MoC^+ ($^2\Delta$)	r(Mo−C)	1.643	1.641	1.619	1.617	1.531	1.527
MoC^+ ($^4\Sigma^+$)	r(Mo−C)	1.700	1.698	1.690	1.687	1.563	1.562
$MoCH^+$ ($^3\Sigma^-$)[a]	r(Mo−C)	1.718	1.718	1.734	1.733	1.608	1.606
	r(C−H)	1.089	1.089	1.080	1.080	1.086	1.087
$MoCH_2^+$ ($^4B_1$)[b]	r(Mo−C)	1.880	1.879	1.920	1.918	1.875	1.885
	r(C−H)	1.094	1.094	1.084	1.084	1.089	1.089
	∠MoCH	121.8	122.0	122.1	122.4	122.9	122.9
$MoCH_3^+$ ($^5A_1$)[c]	r(Mo−C)	2.104	2.098	2.110	2.104	2.020	2.033
	r(C−H)	1.094	1.095	1.086	1.086	1.093	1.094
	∠MoCH	108.8	109.2	108.9	109.2	112.3	112.2

[a] In all cases, the ∠MoCH bond angle is 180°. [b] In all cases, the molecule is planar and has C_{2v} symmetry. [c] In all cases, the molecule has C_{3v} symmetry.

states with excitation energies of 1.61 and 1.09 eV, respectively. Several triplet states are found at energies between 1.6 and 2.1 eV: $^3\Sigma^+$ ($\sigma_b^2\pi^2\delta^2$), $^3\Phi$ ($\sigma_b^2\pi^1\delta^3$), $^3\Pi$ ($\sigma_b^2\pi^1\delta^3$), and $^3\Delta$ ($\sigma_b^2\pi^2\delta^1\sigma^1$), where the latter three spin states exhibit spin contamination ($s^2 = 2.7-3.0$ instead of 2.0).

4.2. MoC^+. The MoC^+ bond energy has been measured previously as 4.31 ± 0.20 eV from the endothermicity of the $Mo^+ + CO \rightarrow MoC^+ + O$ reaction.[22] In the CH_4 system, the threshold obtained from the MoC^+ cross section results in $D_0(Mo^+-C)$ of 4.62 ± 0.11 eV, Table 2. The weighted average of these two values is 4.55 ± 0.19 eV (where the uncertainty is twice the standard deviation of the mean) and is our best experimental value at present.

Theoretically, we find that the ground state of MoC^+ is $^2\Delta$, with a valence configuration (ignoring the C(2s) electrons) of $\sigma_b^2\pi_b^4\delta^1$, where the σ_b and π_b orbitals are Mo−C bonding and the δ orbital is a Mo-based nonbonding orbital. Excited states located include $^4\Sigma^+$ ($\sigma_b^1\pi_b^4\delta^2$), $^2\Sigma^+$ ($\sigma_b^1\pi_b^4\delta^2$), $^4\Phi$ ($\sigma_b^1\pi_b^3\delta^3$), $^2\Gamma$ ($\sigma_b^1\pi_b^4\delta^2$), $^4\Delta$ ($\sigma_b^1\pi_b^4\delta^1\sigma^1$), $^6\Sigma^+$ ($\sigma_b^2\pi_b^2\delta^2\sigma^1$), $^4\Phi$ ($\sigma_b^2\pi_b^3\delta^1\sigma^1$), $^2\Sigma^+$ ($\sigma_b^2\pi_b^4\sigma^1$), and $^2\Delta$ ($\sigma_b^0\pi_b^4\delta^3$), where the additional σ orbital is largely Mo(5s). Excitation energies and bond lengths for each of these states are given in Tables S2 and S3. The relative energy of the $^2\Delta$ and $^4\Sigma^+$ states was checked at several levels of theory, and the former was always found to be the ground state. Excitation energies ranged from 0.173 (BHLYP/SD) to 0.588 eV (QCISD(T)/SD), although the MP2 approach gives much higher values (1.15−1.30 eV), Table S1. Except for the BHLYP approach, which gives a MoC^+ ($^2\Delta$) bond energy much lower than experiment, the B3LYP, MP2, and QCISD(T) values ranged from 3.96 to 4.39 eV with the SD basis on Mo consistently giving higher values than HW by an average of 0.22 ± 0.04 eV, Table 3. The HW* basis set performs similarly to SD with values higher than HW by an average of 0.17 ± 0.05 eV, Table 3. The higher values obtained (MP2/SD and QCISD(T)/SD) agree with the experimental results within the experimental uncertainty.

4.3. $MoCH^+$. The threshold obtained for the $MoCH^+$ cross section results in $D_0(Mo^+-CH)$ of 5.12 ± 0.30 eV, Table 2. In related work on the reactions of Mo^+ with C_2H_6 and C_3H_8 we obtain BDEs for Mo^+-CH of 5.29 ± 0.10 and 5.38 ± 0.11 eV, respectively.[65] Our best value for $D_0(Mo^+-CH)$ is the weighted average of all three values, yielding 5.32 ± 0.14 eV, where the uncertainty is two standard deviations of the mean.

Theory finds a $^3\Sigma^+$ ground state with a $\sigma_b^2\pi_b^4\delta^2$ electron configuration, where the character of the orbitals is the same as MoC^+. Thus, a covalent triple bond is formed leading to a linear geometry. Excited states (all calculated to lie >0.9 eV higher in energy) include $^1\Gamma$ ($\sigma_b^2\pi_b^4\delta^2$), $^3\Delta$ ($\sigma_b^2\pi_b^4\delta^1\sigma^1$), $^1\Delta$ ($\sigma_b^2\pi_b^4\delta^1\sigma^1$), and $^1\Sigma^+$ ($\sigma_b^2\pi_b^4\sigma^2$). Excitation energies and bond lengths are given in Tables S2 and S3, respectively. As for

MoC^+, the BHLYP functional does not predict a bond energy close to experiment, whereas the other levels of theory yield bond energies ranging from 4.03 to 4.92 eV, Table 3. Again, the HW* and SD basis sets yield bond energies higher than those for HW by averages of 0.13 ± 0.07 and 0.15 ± 0.06 eV, respectively. The highest of these values (B3LYP/SD, QCISD(T)/HW*, and QCISD(T)/SD) are slightly below the experimental value obtained above.

The $HMoC^+$ isomer was also examined to ensure that the linear molybdenum carbyne cation was indeed the ground-state structure. The lowest energy species was a $^1A'$ having a bond angle of 85.5° and lying 2.46 eV above $MoCH^+$ ($^3\Sigma^+$). The lowest triplet state of this isomer, $^3A''$, lies only 0.06 eV above the $^1A'$ state, and a $^3A'$ state lies another 0.57 eV higher, Table S2.

4.4. $MoCH_2^+$. The dominant reaction in the methane systems is the endothermic dehydrogenation reaction 5. Our measurements of the threshold for reaction 5 result in $D_0(Mo^+-CH_2) = 3.57 \pm 0.10$ eV. This product is also observed in endothermic reactions of Mo^+ with ethane and propane.[65] In these systems, the thresholds obtained can be converted to Mo^+-CH_2 bond energies of 2.90 ± 0.13 and 3.57 ± 0.12 eV, respectively. The latter value helps confirm the accuracy of the value determined in the methane system, whereas the discrepancy with the ethane result suggests that this reaction is limited by a barrier in excess of the endothermicity.

Bauschlicher et al.[28] calculated the properties of the ground states of the MCH_2^+ molecules using a modified coupled-pair functional (MCPF) approach followed by complete-active-space SCF (CASSCF)/internally contracted averaged CPF (ICACPF) single-point calculations, all using the Hay−Wadt ECP on molybdenum. They predict a $^4B_1$ ground state having a Mo−C bond distance of 1.888 Å and a MoCH bond angle of 121.6°. This state corresponds to a valence electron configuration of $(1a_{1b})^2(1b_{1b})^2(2a_1)^1(1a_2)^1(1b_2)^1$, where the $1a_{1b}$ and $1b_{1b}$ orbitals are the Mo−C σ and π bonds and the remaining orbitals are metal-based nonbonding 4d orbitals. At the MCPF level, this species is found to have a Mo^+-CH_2 bond energy (D_e) of 2.70 eV, which increases to 2.91 eV at the ICACPF level. The final "best estimate" of $D_0 = 3.08 \pm 0.17$ eV includes corrections for zero-point motion (−0.09 eV), limitations in the correlation treatment ($+0.04 \pm 0.04$ eV), and basis-set incompleteness ($+0.22 \pm 0.17$ eV). This value lies somewhat below the experimental bond energy measured here of 3.57 ± 0.10 eV. A similar discrepancy is observed for the neighboring element, where we measured an experimental bond energy of 4.44 ± 0.09 eV for $NbCH_2^+$,[17] whereas the calculations of Bauschlicher et al.[28] provide a "best estimate" of 3.86 ± 0.13 eV.

Our calculations also find a $^4B_1$ state for $MoCH_2^+$, with a very similar geometry (Table 4). B3LYP and QCISD(T) bond energies for this species range from 2.96 to 3.44 eV, whereas the BHLYP and MP2 values run from 2.55 to 2.73 eV, Table 3. Again the HW* and SD basis sets yield higher values by 0.14 ± 0.09 and 0.20 ± 0.08 eV compared to the HW basis. Our calculated values agree well with the best estimate of Bauschlicher et al.,[28] and the B3LYP and QCISD(T) values using the HW* and SD basis sets are in reasonable agreement with the experimental value. The BHLYP and MP2 values are much too low, as previously found for the BHLYP functional with the first-row transition-metal carbene cations.[61] The only possible means of lowering the experimentally determined BDE is if there are unaccounted sources of reactant energy. This cannot be higher energy spin−orbit states as the ^6S ground state has none nor can it be excited electronic states of Mo^+ as even the first excited state (^6D at 1.587 eV) is much too high in energy to account quantitatively for the discrepancy observed. Furthermore, there is no evidence for such an excited state in other reaction channels or in our previous results for reactions with H_2, D_2, and CO.[21,22]

Our calculations also find excited quartet states of $^4B_2$ $[(1a_{1b})^2(1b_{1b})^2(2a_1)^1(1b_2)^1(3a_1)^1]$ (where the $3a_1$ orbital is largely Mo 5s) at 1.13 eV, $^4A_1$ $[(1a_{1b})^2(1b_{1b})^1(2a_1)^2(1a_2)^1(1b_2)^1]$ at 1.82 eV, $^4A_1$ $[(1a_{1b})^2(1b_{1b})^1(2a_1)^1(1a_2)^1(1b_2)^1(3a_1)^1]$ at 2.11 eV, and $^4A_2$ $[(1a_{1b})^2(1b_{1b})^1(2a_1)^2(1a_2)^0(1b_2)^1(3a_1)^1]$ at 2.66 eV. Doublet states of $^2B_1$ $[(1a_{1b})^2(1b_{1b})^2(2a_1)^1(1a_2)^1(1b_2)^1]$ at 0.73 eV, $^2B_2$ $[(1a_{1b})^2(1b_{1b})^2(2a_1)^2(1a_2)^0(1b_2)^1]$ at 1.37 eV, $^2A_2$ $[(1a_{1b})^2(1b_{1b})^2(2a_1)^2(1a_2)^1(1b_2)^0]$ at 1.26 eV (which has an imaginary frequency such that it collapses to the $^2B_1$ state), and $^2A_1$ $[(1a_{1b})^2(1b_{1b})^1(2a_1)^2(1a_2)^0(1b_2)^0(3a_1)^1]$ at 2.10 eV were also located. We also found two high-spin sextet states: $^6A_1$ $[(1a_{1b})^2(1b_{1b})^1(2a_1)^1(1a_2)^1(1b_2)^1(3a_1)^1]$ at 0.84 eV and $^6B_1$ $[(1a_{1b})^1(1b_{1b})^2(2a_1)^1(1a_2)^1(1b_2)^1(3a_1)^1]$ at 2.61 eV. Details can be found in Tables S2 and S3.

Because of the possibility of different isomers, as observed for several other transition-metal carbenes such as WCH_2^+,[44] we also examined the $HMoCH^+$ molecule, finding a ground state of $^2A''$ symmetry lying 0.724 eV higher in energy than the $MoCH_2^+$ ($^4B_1$) ground state. Excited states for this species include $^2A'$ and $^4A'$, located 1.11 and 1.93 eV above $MoCH_2^+$ ($^4B_1$). Geometries for these various states are given in Table S3.

4.5. $MoCH_3^+$. The threshold obtained for the $MoCH_3^+$ cross section in the CH_4 system results in $D_0(Mo^+-CH_3) = 1.44 \pm 0.11$ eV, Table 2. Given that the threshold for MoH^+ in this system was shifted to higher energies because of competition with the dehydrogenation reaction, a better estimate of the Mo^+-CH_3 bond energy comes from taking the relative thresholds for MoH^+ and $MoCH_3^+$ (0.09 ± 0.12 eV, Table 2) and subtracting this from $D_0(Mo^+-H) = 1.72 \pm 0.06$ eV. This yields $D_0(Mo^+-CH_3) = 1.63 \pm 0.12$ eV. Values of 1.45 ± 0.08 and 1.62 ± 0.06 eV are obtained from comparable results obtained in the reactions of Mo^+ with C_2H_6, and C_3H_8, respectively.[65] The weighted average of these three values is 1.57 ± 0.09 eV (2 standard deviations of the mean), which compares well with the theoretical value of 1.38 ± 0.13 eV given by Bauschlicher et al.[29] and somewhat higher than that calculated Schilling et al.[30] of 1.31 eV. This agreement identifies this species as the molybdenum methyl cation having a $^5A_1$ ground state. Our own calculations find bond energies ranging from 1.32 to 1.89 eV with the HW* and SD basis sets giving values exceeding the HW results by averages of 0.07 ± 0.05 and 0.13 ± 0.02 eV, Table 3. As found previously by Holthausen et al. for first- and third-row transition-metal methyl cations,[60] the B3LYP functional tends to overbind as does the QCISD(T) method. The BHLYP and MP2 approaches provide bond energies in reasonable agreement with experiment and previous theoretical results.

Our calculations agree that $MoCH_3^+$ has a $^5A_1$ ground state, but we also find a $^3A'$ state lying 0.99 eV higher in energy. Whereas the $^5A_1$ state has C_{3v} symmetry and three equal MoCH bond angles of 108.8°, the $^3A'$ state has a weak agostic interaction such that the MoCH bond angles are 107.5° (2) and 111.9°. Fairly close in energy (0.07 and 0.13 eV above the $^3A'$ state) lie the $^3A''$ and ^3A states of $HMoCH_2^+$ and H_2MoCH^+, respectively. The lowest energy singlet species, $^1A'$, also has the H_2MoCH^+ structure and lies 1.72 eV higher than the $^5A_1$ state. Geometries of these various species are detailed in Table S3.

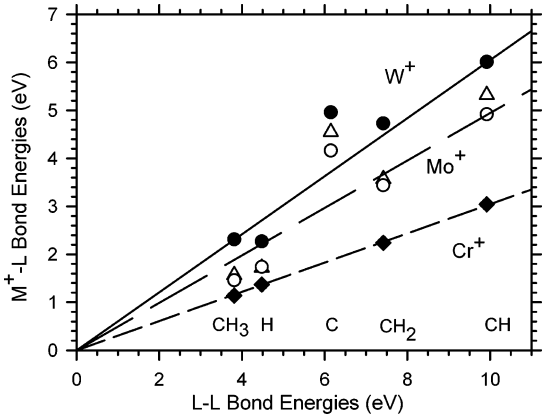

Figure 2. Correlation of Mo^+-L bond energies with those for the organic analogues, L−L. Mo^+-L values are from Table 3 and include both experiment (open triangles) and theory (open circles; BHLYP/SD/6−311++G(3df,3p) for MoH^+ and $MoCH_3^+$ and B3LYP/SD/6-311++G(3df,3p) for all others). The long dashed line is a linear regression fit to the experimental data, excluding Mo^+-C, constrained to pass through the origin to emphasize the bond-order correlations. Data for CrL^+ and WL^+ (taken from refs 7, 43, 44, and 67−70) are shown by closed diamonds and circles, respectively, and the short dashed and full lines are linear regression fits to these data.

4.6. Bond-Energy Bond-Order Correlation for Mo^+-CH_x Bonds. One interesting way of investigating the bond order of simple metal−ligand species is to compare with organic analogues, i.e., $D_0(Mo^+-L)$ vs $D_0(L-L)$.[66] Such a plot is shown in Figure 2, where it can be seen that the correlation is reasonably good except for MoC^+. (This regression line is constrained to include the origin to emphasize the bond-order correlation of the MoL^+ vs L_2 species.) The good correlation indicates that Mo^+-H and Mo^+-CH_3 are both single bonds, $Mo^+=CH_2$ is a double bond, and $Mo^+\equiv CH$ is a triple bond, all in agreement with theoretical characterizations as well. The point that lies furthest from the line is for Mo^+-C, correlated with the BDE of C_2. In this case, the MoC^+ BDE lies above the line because the covalent double bond in this molecule can be augmented by back-donation of an occupied 4dπ orbital on Mo^+ into the empty 2pπ orbital on C, an interaction that cannot occur in the C_2 molecule. Also illustrated in Figure 2 is the relatively good agreement between experiment and theory: B3LYP/SD for multiply bonded species and BHLYP/SD for the singly bonded species. Examination of Table 3 shows that the best overall theoretical treatment is the QCISD(T) method with either the HW* or the SD basis set, where the mean absolute deviation (MAD) from experiment is 0.26 eV, but the B3LYP method with either of these basis sets is nearly as accurate.

Figure 2 also compares the bond energies determined here for Mo^+ with those previously measured for the other group 6 metal ions, Cr^+ and W^+. The values for the other two congeners are $D_0(Cr^+-H) = 1.37 \pm 0.09$ eV,[7,67] $D_0(Cr^+-CH_3) = 1.14 \pm 0.03$ eV,[7,68,69] $D_0(Cr^+-CH_2) = 2.24 \pm 0.04$ eV,[7,43,69] $D_0(Cr^+-CH) = 3.04 \pm 0.30$ eV,[7,69] $D_0(W^+-H) = 2.27 \pm 0.05$ eV,[70] $D_0(W^+-CH_3) = 2.31 \pm 0.10$ eV, $D_0(W^+-CH_2) = 4.74 \pm 0.03$ eV, $D_0(W^+-CH) = 6.01 \pm 0.28$ eV, and $D_0(W^+-C) = 4.96 \pm 0.22$ eV.[44]

The BDEs for Mo^+ are intermediate between those of Cr^+ and W^+, which can be explained by considering promotion energies and s- and d-orbital sizes.[71−74] The ground state of W^+ is $6s^15d^4$ (^6D), a configuration suitable for forming a strong single covalent bond as well as multiple covalent bonds, whereas Cr^+ and Mo^+ have ^6S (d^5) ground states. Their promotion energies to ^6D (s^1d^4) excited states are 1.48 and 1.46 eV, respectively.[64] In W^+, relativistic effects cause the 6s orbital to shrink so that its radial extent closely matches that of the 5d orbitals, thereby allowing more effective hybridization of these orbitals. Irikura and Beauchamp reported that the orbital size differences between valence s and d orbitals decrease from Cr^+ to Mo^+ to W^+.[71] This helps explain why Mo^+ shows stronger bond strengths than Cr^+, even though promotion energies are similar for Cr^+ and Mo^+.

5. Discussion

5.1. Reaction Mechanism. As noted above, there is strong competition observed between the formation of the thermodynamically favored products, $MoCH_2^+ + H_2$, and the $MoH^+ + CH_3$ products. A key observation is that the decline in the $MoCH_2^+$ cross section is compensated by the increase in the MoH^+ cross section, Figure 1. Although contributions of direct abstraction processes to the formation of MoH^+ cannot be excluded (see below), such a mechanism is unlikely to compete so efficiently with the dehydrogenation channel. However, if reactions 2 and 5 share a common intermediate and $MoH^+ + CH_3$ formation is kinetically favored, then this process can rapidly deplete the intermediate before the more complicated dehydrogenation reaction can occur at sufficiently high energies. This competition is readily explained by formation of an $H-Mo^+-CH_3$ intermediate, which can be formed by an oxidative addition mechanism in which M^+ inserts into a C−H bond of methane.[1,5,9] MoH^+ formation can occur from this intermediate by simple bond cleavage at elevated kinetic energies, whereas H_2 elimination must occur by a more restricted transition state, which is not obviously elucidated by the experimental results alone.

The H_2 elimination processes can occur either by multicenter transition states or by rearrangement of the intermediate through a β-H transfer to form $(H)_2MCH_2^+$ species, which then reductively eliminate H_2. Among the key issues in determining the detailed mechanism is the spin states of the reactant, intermediates, and products and the stabilities of two types of possible intermediates: $H-Mo^+-CH_3$ and $(H)_2MoCH_2^+$. The reactants have a sextet spin state, $Mo^+(^6S) + CH_4$ ($^1A_1$). Calculations (in all cases, confirmed by the present work) indicate that the ground state of MoH^+ is $^5\Sigma^+$,[25,26] $MoCH_3^+$ is $^5A_1$,[29] $MoCH_2^+$ is $^4B_1$,[28] and $H-Mo^+-CH_3$ is $^4A'$.[12] Thus, formation of the $MoH^+ + CH_3$ and $MoCH_3^+ + H$ products is spin allowed, whereas formation of $MoCH_2^+ + H_2$ products and the $H-Mo^+-CH_3$ intermediate is spin forbidden. Additionally, the possible $(H)_2MoCH_2^+$ intermediate will have a doublet ground state presuming that the MoH bonds are covalent and there is a MoC double bond, a result confirmed by the present calculations. This indicates that there is a change in spin from sextet to quartet as the reactants interact strongly with methane to form the $H-Mo^+-CH_3$ intermediate. If the dihydride intermediate is important in the dehydrogenation process, then two more spin changes (quartet−doublet−quartet) may be necessary. To elucidate the mechanism for dehydrogenation further, we turn to theory.

In the following sections, the energies (including zero-point energies) and structures of the reactants, products, and intermediates on the sextet, quartet, and doublet potential-energy surfaces were calculated using the B3LYP/HW (B3LYP/SD) level of theory, which from Table 3 can be seen to provide reasonable agreement with the experimental values at a modest computational cost. The B3LYP/HW energies are shown graphically in Figure 3, and structures are shown in Figures 4−6. Details of our theoretical calculations can be found in the

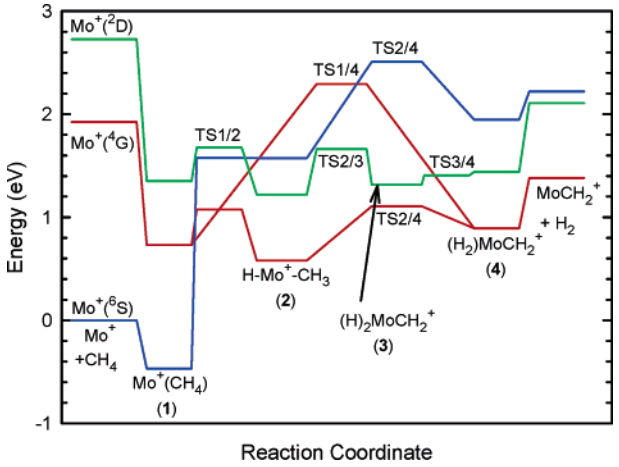

Figure 3. $[Mo,C,4H]^+$ potential-energy surfaces derived from theoretical results. The energies of all species relative to the Mo^+ (^6S) + CH_4 ground-state asymptote are based on ab initio calculations (B3LYP/HW/6-311++G(3df,3p), see Table S4).

Supporting Information, which provides both energies (Table S4) and structures (Table S5) of all species.

5.2. Sextet Potential-Energy Surface. Previously, Blomberg et al. characterized the ground state of the $Mo^+(CH_4)$ complex (**1**) formed by condensation of methane with the atomic molybdenum cation.[12] They determine a $^6A_1$ ground state lying 0.38 eV below the reactants and having a Mo−C bond length of 2.80 Å. Our present B3LYP/HW (B3LYP/SD) calculations find binding energies of 0.47 (0.56) eV with bond lengths of 2.642 (2.594) Å. This molecule has C_{2v} symmetry in which the metal ion bisects one of the HCH bond angles (η^2 binding). As noted by Blomberg et al., Mo^+ binds methane somewhat more weakly than other second-row metal ions because of its half-filled high-spin 4d shell, which requires that there is an occupied 4d orbital pointing at the ligand.

After formation of $Mo^+(CH_4)$, activation of a C−H bond on the sextet surface leads to an H−Mo^+−CH_3 ($^6A'$) intermediate (**2**) via TS1/2 ($^6A'$), Figure 4. Because of the high spin, this intermediate cannot have a covalent bond with both H and CH_3, such that the Mo−C bond distance is quite long, 2.535 (2.523) Å. The transition state has a very similar geometry, r(Mo−C) = 2.528 (2.512) Å, and its energy is only 0.002 (0.007) eV higher than the intermediate (including zero-point energy corrections). The H−Mo^+−CH_3 ($^6A'$) intermediate lies well above, by 1.00 (1.06) eV, the quartet ground state for this species. Elimination of H_2 from this intermediate can proceed over TS2/4 ($^6A'$), a four-centered transition state lying 0.94 (0.90) eV higher in energy. TS2/4 leads to the sextet dihydrogen molybdenum carbene ion, $(H_2)MoCH_2^+$ ($^6A'$) (**4**), lying 1.95 (1.63) eV above the reactants. The dihydrogen molecule is weakly bound as it requires only 0.27 (0.31) eV to form $MoCH_2^+$ ($^6A_1$) + H_2, a process that is endothermic by 2.22 (1.94) eV overall.

5.3. Quartet Potential-Energy Surface. The excited ^4G state of Mo^+ interacts more strongly with methane than the sextet ground state because the low spin allows electron density on the metal ion to be moved from the intermolecular bonding axis. The Mo^+−CH_4 bond energy in the $^4A_1$ state is 1.19 (1.29) eV, but this species still lies above ground-state reactants by 0.73 (0.60) eV. Activation of a CH bond through TS1/2 ($^4A'$) leads to the $^4A'$ ground state for the H−Mo^+−CH_3 intermediate (**2**). TS1/2 is found here to lie 1.08 (0.83) eV above the ground-state reactants. This agrees reasonably well with the previous theoretical results of Blomberg et al., who calculated the energy

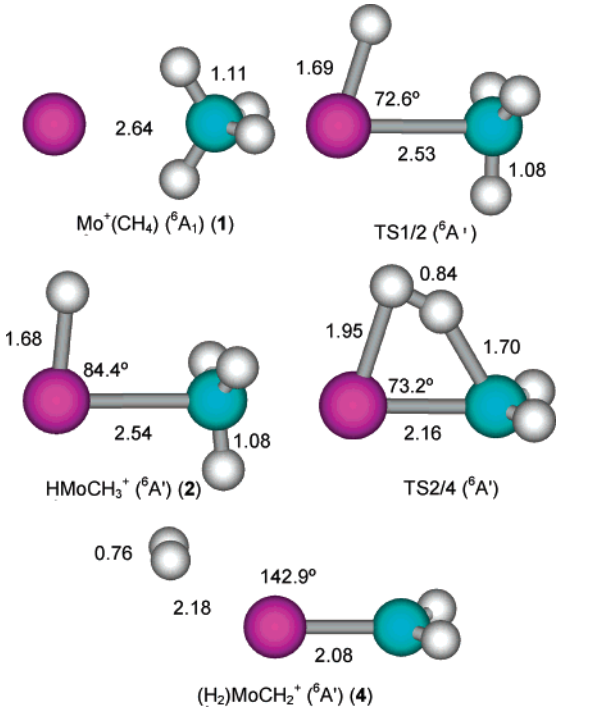

Figure 4. Structures of several intermediates and transition states along the sextet surface of the $[Mo,C,4H]^+$ system calculated at the B3LYP/HW/6-311++G(3df,3p) level of theory. Bond lengths are given in Å and HMoC bond angles in deg.

of this transition state as 1.21 eV (1.90 eV before an empirical correction for zero point, basis set, and correlation effects).[12] Their geometry, r(Mo−H) = 1.69 Å, r(Mo−C) = 2.16 Å, and ∠HMoC = 49.6°, differs somewhat from that found here at the B3LYP/HW (SD) levels: 1.769 (1.796) Å, 2.084 (2.043) Å, and 40.8 (40.5) °, respectively.

In the H−Mo^+−CH_3 intermediate, both the Mo−H, 1.677 (1.681) Å, and Mo−C, 2.063 (2.057) Å, bond lengths are comparable to those found in the covalently bound MoH^+, 1.673 (1.676) Å, and $MoCH_3^+$, 2.104 (2.098) Å, species. The HMoC bond angle is 113.5° (112.8°). Blomberg et al.[12] obtain similar bond lengths, 1.68 and 2.08 Å, respectively, and bond angles, 112.2°. The energy of this intermediate is calculated to lie 0.58 (0.31) eV above the reactants, somewhat lower than the energy calculated by Blomberg et al. of 0.77 eV (1.46 eV before an empirical correction for zero-point, basis set, and correlation effects).

As on the sextet surface, the H−Mo^+−CH_3 intermediate can rearrange via a four-centered transition state, TS2/4 ($^4A'$), to form $(H_2)MoCH_2^+$ ($^4A'$) (**4**), lying 0.89 (0.64) eV above ground-state reactants. Loss of H_2 requires an additional 0.49 (0.58) eV of energy to form the ground-state products, $MoCH_2^+$ ($^4B_1$) + H_2, in a process calculated to be endothermic overall by 1.38 (1.22) eV relative to ground-state reactants. (Relative to the Mo^+(^4G) + CH_4 reactants, the reaction is calculated to be exothermic by 0.54 (0.67) eV.) These values compare favorably with the experimental endothermicity of 1.14 ± 0.10 eV, Table 2. Note that both TS1/2 ($^4A'$) and TS2/4 ($^4A'$) are calculated to lie below the energy of the product asymptote, by 0.31 (0.39) and 0.27 (0.42) eV, respectively, such that the energy-limiting step along the quartet potential-energy surface corresponds to product formation. Blomberg et al.[12] calculated that the elimination of H_2 from H−Y^+−CH_3 occurs by passing over a four-center transition state, calculated to lie about 0.43 eV below the energy of the products. They reasonably assumed that a similar mechanism is followed for the other second-row metal

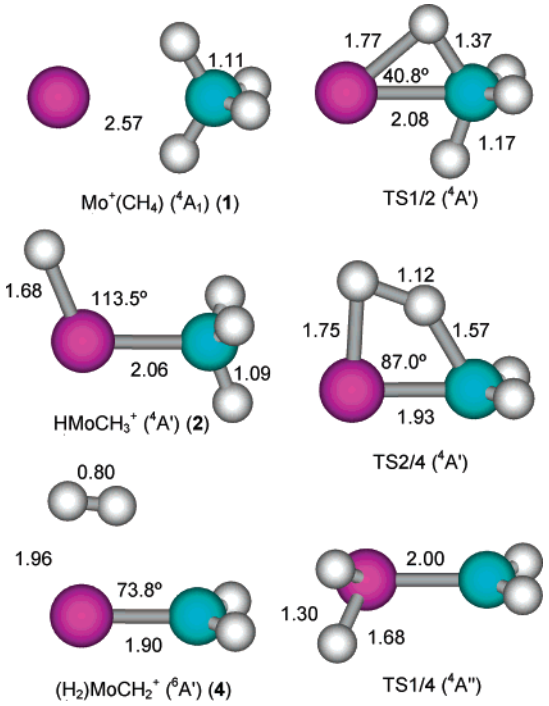

Figure 5. Structures of several intermediates and transition states along the quartet surface of the $[Mo,C,4H]^+$ system calculated at the B3LYP/HW/6-311++G(3df,3p) level of theory. Bond lengths are given in Å and HMoC bond angles in deg.

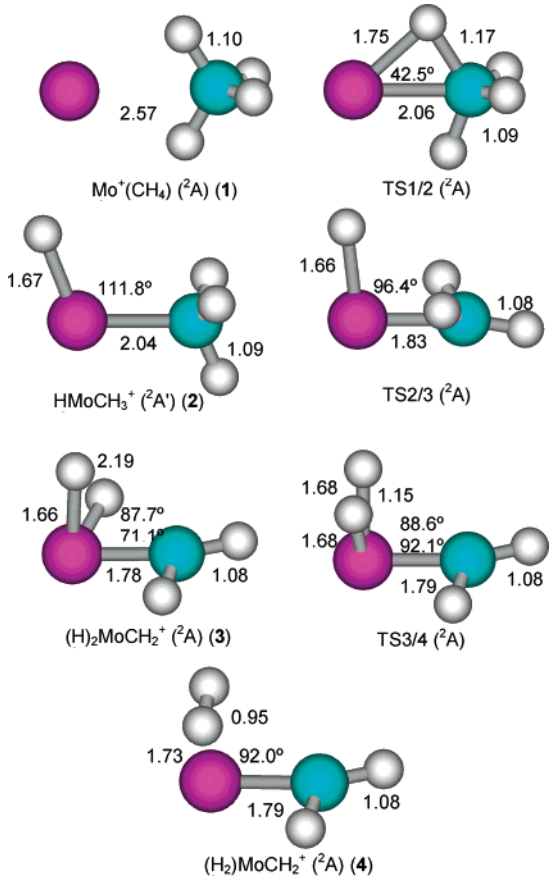

Figure 6. Structures of several intermediates and transition states along the doublet surface of the $[Mo,C,4H]^+$ system calculated at the B3LYP/HW/6-311++G(3df,3p) level of theory. Bond lengths are given in Å and HMoC bond angles in deg.

ions and that the relative energetics are not that different. Our explicit calculations indicate the veracity of this assumption for molybdenum.

An alternate pathway for dehydrogenation was also discovered while searching for the dihydride molybdenum carbene cation on the quartet surface, a species never located. We did find, however, that two C−H bonds in the $Mo^+(CH_4)$ complex could be simultaneously activated and lead directly to the $(H_2)MoCH_2^+$ intermediate. This TS1/4 ($^4A''$) species has not been characterized previously for other metals, and no analogue on the sextet or doublet surfaces was located either. The energy of this transition state is well above that for the other pathway on the quartet surface, lying 2.29 (1.94) eV above the ground-state reactants.

5.4. Doublet Potential-Energy Surface. A variety of intermediates and transition states were also examined on the doublet potential-energy surface. The $Mo^+(CH_4)$, $H-Mo^+-CH_3$, and $(H_2)MoCH_2^+$ intermediates as well as TS1/2 were all located and found to lie above the quartet analogues by similar energies: 0.62 (0.63), 0.64 (0.63), 0.55, and 0.60 (0.60) eV, respectively. This energy separation is similar to that for the product asymptote, $MoCH_2^+$ ($^2B_1$) + H_2, which lies 0.73 (0.72) eV above the ground-state $MoCH_2^+$ ($^4B_1$) + H_2 products, and to the separation between the ^4G and ^2D Mo^+ atomic states, 0.80 (0.91), which agree well with the experimental splitting of 0.90 eV.[64] Despite careful searches, neither TS2/4 nor TS1/4 could be located on the doublet surface. Instead, dehydrogenation of $H-Mo^+-CH_3$ occurs by a stepwise process in which the dihydride molybdenum carbene cation, $(H)_2MoCH_2^+$ (^2A) (**3**), is formed over TS2/3 (^2A) and then reductive elimination of H_2 over TS3/4 (^2A) occurs to form $(H_2)MoCH_2^+$ (^2A). These are all relatively low-energy steps but nevertheless continue to lie above the energy of the quartet surface throughout the transformation. Interestingly, the energy of TS3/4 (^2A) is actually lower than that of $(H_2)MoCH_2^+$ (^2A) by 0.033 eV but higher by 0.012 eV before zero-point energy corrections at the B3LYP/HW level. (Indeed, calculations of TS3/4 at the B3LYP/SD level would not converge. B3LYP/SD calculations starting at the geometry of $(H_2)MoCH_2^+$ (^2A) collapsed to a rotamer of the $(H)_2MoCH_2^+$ (^2A) intermediate.) Thus, interaction of $MoCH_2^+$ ($^2B_1$) with H_2 should spontaneously form the $(H)_2MoCH_2^+$ (^2A) dihydride with no intermediate barriers.

5.5. Dehydrogenation. Armed with the potential-energy surfaces of Figure 3, the mechanism for the dehydrogenation of methane by Mo^+ (^6S) is clear. Formation of $MoCH_2^+$ at its experimental threshold of 1.14 ± 0.10 eV must correspond to formation of ground-state $MoCH_2^+$ ($^4B_1$) + H_2 ($^1\Sigma_g^+$) products. Therefore, there must be a crossing from the sextet spin surface of the reactants to the quartet spin surface of the products. Remaining on the sextet surface for TS1/2 and beyond requires too much energy as does any involvement of the doublet surface. In contrast, on the quartet surface, the energies of neither TS1/2 nor TS2/4 exceed the energy of the product asymptote. Thus, reaction must occur by initial formation of the ground-state $Mo^+(CH_4)$ ($^6A_1$) complex, coupling to the quartet surface as oxidative addition of the C−H bond to the metal center occurs to form $H-Mo^+-CH_3$ ($^4A'$). Four-centered reductive elimination of dihydrogen produces $(H_2)MoCH_2^+$ ($^4A'$), from which the loosely bound H_2 molecule is easily lost.

Further insight into the four-centered reductive elimination step can be obtained by considering the reverse reaction, i.e., H_2 activation by $MoCH_2^+$. The following discussion is consistent with simple molecular orbital ideas developed for the activation of H_2 and CH_4 by metal oxide ions.[75] As discussed in detail elsewhere,[1,2] activation of covalent bonds at transition-metal centers is most facile when the metal has an empty s-like

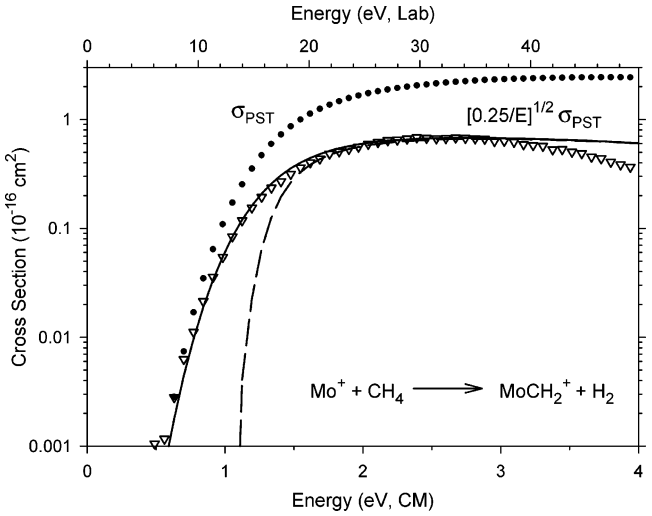

Figure 7. Experimental dehydrogenation cross section (open triangles) compared to the cross section calculated using phase space theory (PST) (dots) and then adjusted for the probability of crossing between surfaces of different spin (full line). These theoretical results have been convoluted over the energy distributions of the reactants, whereas the dashed line shows the latter prediction without this convolution.

valence orbital to accept the pair of electrons in the covalent bond and when it has a pair of valence dπ-like electrons to donate into the antibonding orbital of the bond to be broken. For the metal carbenes, the valence molecular orbitals (MOs) are $1a_{1b}$ and $1b_{1b}$ M−C bonding; $2a_1$, $1a_2$, and $1b_2$ 4d-like nonbonding; a $3a_1$ 5*s*-like nonbonding; and $2b_1$* and $4a_1$* antibonding orbitals. For these species, the most likely acceptor orbital is the $3a_1$ MO and the π-donor orbital is one of the three 4d-like nonbonding MOs. The $^4B_1$ ground state of $MoCH_2^+$ has a $(1a_{1b})^2(1b_{1b})^2(2a_1)^1(1a_2)^1(1b_2)^1(3a_1)^0$ valence electron configuration.[28] Because this state does not occupy the $3a_1$ acceptor orbital, the interaction of $MoCH_2^+$ ($^4B_1$) with H_2 is attractive and allows facile activation of H_2 across the Mo−C bond to form H−Mo^+−CH_3. Thus, TS2/4 lies below the product asymptote. In contrast, the $MoCH_2^+$ ($^6A_1$) state has a $(1a_{1b})^2(1b_{1b})^1(2a_1)^1(1a_2)^1(1b_2)^1(3a_1)^1$ valence electron configuration, leading to a more repulsive interaction with H_2. Thus, the sextet state of TS2/4 lies well above its respective product asymptote, Figure 3. Not surprisingly, the $^2B_1$ state, which has the same electron configuration as the $^4B_1$ state, also efficiently activates the H_2 bond, but in this case, the low-spin state allows the donor orbital to become doubly occupied during the addition process. This allows two covalent bonds to Mo^+ to be formed, yielding the dihydride $(H)_2MoCH_2^+$ (^2A) intermediate directly.

5.6. Efficiency of Spin Changes. In an attempt to provide a quantitative measure of the efficiency of the sextet−quartet surface coupling, we modeled the experimental $MoCH_2^+$ cross section using a phase space theory (PST) approach with molecular parameters (vibrational and rotational constants) calculated here. Using statistical assumptions and rigorous angular momentum conservation, these calculations determine an absolute magnitude for the cross section using the Langevin−Gioumousis−Stevenson (LGS) collision limit.[76] Hence, the only adjustable parameter in the PST calculation is the endothermicity for reaction 5, $E_0(5)$. The PST modeling utilizes $E_0(5) = 1.05$ eV, slightly below the optimum threshold value determined using an analysis of the experimental cross section with eq 1, Table 2. We find that the PST modeling reproduces the experimental cross section at threshold but that it rapidly becomes too large, Figure 7. Interestingly, the deviation between the experimental and PST cross sections has an energy dependence of approximately $E^{1/2}$, which can be rationalized by the energy dependence for crossing between surfaces of different spin multiplicity. As discussed in detail elsewhere,[77] it has been shown that the statistical limit for the crossing probability between diabatic surfaces of different spin multiplicities can be described using a Landau−Zener model,[78,79] which gives the probability as approximately $P_{LZ} = [c/(E - E_c)]^{1/2}$, where E is the total energy available to the system (here essentially the translational energy of the reactants), c is a surface coupling term that depends on the energy gap between the adiabatic curves and inversely on the difference in the slopes of the diabatic curves at the crossing point, and E_c is the potential energy of the crossing point.[80,81] As long as the value of E_c is below the threshold for reaction, the difference between $[c/(E - E_c)]^{1/2}$ and $[c/E]^{1/2}$ is rather small (as verified here). The comparison between the cross sections determined experimentally, calculated using phase space theory, and the PST calculation multiplied by $[c/E]^{1/2}$, where $c = 0.25$, is shown in Figure 7. The key conclusion from this comparison is qualitative, namely, the kinetic-energy dependence of the dehydrogenation reaction cross section reflects the need to couple between surfaces of differing spin, such that spin is at least a partially conserved quantity for this second-row transition-metal ion. This result is in contrast to a parallel calculation made for the dehydrogenation of methane by Re^+ where three changes in spin are necessary for reaction to occur.[74] Here, phase space theory was able to account for the energy dependence and the magnitude (within 20%) of the experimental cross section *without* including the $E^{-1/2}$ energy dependence for spin changes. This appears to indicate that spin is essentially no longer a good quantum number in this heavy atom system.

One possible reason that the molybdenum system is sensitive to the spin change (i.e., weak coupling between the surfaces) is related to the nature of the surface intersection. Although it is beyond the scope of this study to examine the details of the crossing seam between the sextet and quartet states, we did investigate this possibility using the following approach. Starting at TS1/2, intrinsic reaction coordinate calculations were conducted on both the quartet and sextet potential-energy surfaces. Once these geometries were obtained, the vertical excitation energies on the surface of differing spin were then calculated at the same geometries. This comparison suggests that the lowest energy intersection point occurs just past ^{4}TS1/2 at an energy very similar to this transition state. (This can be understood because the molecule is very floppy on the sextet surface, a result of the inability of Mo^+(^{6}S) to form a covalent bond to both H and CH_3 simultaneously. Thus, large variations in geometry on the sextet surface do not require a great deal of energy.) This calculation finds that the slopes of the quartet and sextet curves in the region near this intersection are nearly orthogonal, limiting the ability of the surfaces to couple with one another.

5.7. High-Energy Products. At higher energies, the H−Mo^+−CH_3 intermediate decomposes by cleavage of the Mo−H and Mo−C bonds to form the primary $MoCH_3^+$ and MoH^+ products. Although these channels have similar energetics, the latter product is greatly favored as it can conserve angular momentum more easily.[82] At higher energies, MoC^+ and $MoCH^+$ are formed by subsequent dehydrogenation and H-atom loss processes from the primary $MoCH_2^+$ and $MoCH_3^+$ products. The thermochemistry determined above, Table 3, shows that dehydrogenation of these species requires 2.37 ± 0.22 and 0.77 ± 0.15 eV, respectively. The large difference is because the formal bond order changes little in going from Mo^+=CH_2 to Mo^+=C

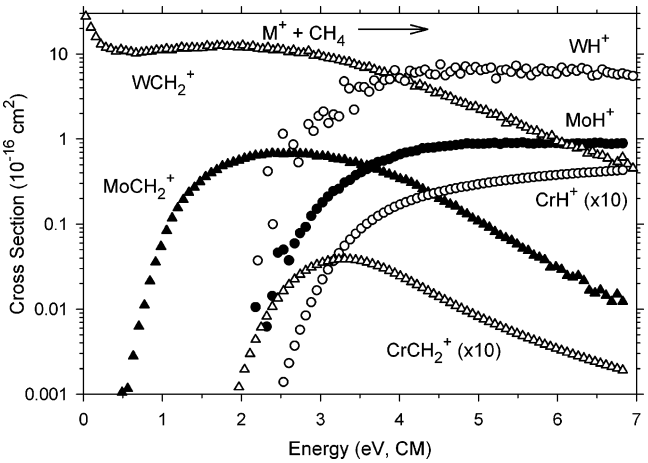

Figure 8. Reactivity of Cr^+, Mo^+, and W^+ with methane compared for the MH^+ and MCH_2^+ products. Data for chromium is a representation of the original data published in ref 43, and that for tungsten is from ref 44.

but changes from 1 to 3 in the transition from Mo^+-CH_3 to $Mo^+\equiv CH$. Further, we note that H-atom loss from $MoCH_3^+$, which can form $MoCH_2^+$, requires 2.64 ± 0.12 eV. Thus, the overall formation of $MoCH_2^+ + 2H$ cannot begin until 5.68 ± 0.16 eV, which makes this process barely accessible on the energy scale examined here, Figure 1.

5.8. Reactivity Differences between Mo^+, Cr^+, and W^+. The kinetic-energy dependence of the reaction of Cr^+ (the first-row transition-metal congener of Mo^+) with CH_4 has been studied previously,[41−43] and recently reactions of W^+, the third-row congener, have also been examined.[44] Simplified versions of these results are compared in Figure 8 with the present data for Mo^+. This comparison makes it clear that the efficiencies of the dehydrogenation processes differ dramatically among the three metals, with the reactivity increasing by a couple of orders of magnitude for each step down the periodic table. This is partly because the reaction is exothermic for W^+, somewhat endothermic for Mo^+, and more so for Cr^+. This result contrasts somewhat with the observations for formation of MH^+, where the energy dependence of all three cross sections is fairly similar, although the absolute magnitudes differ by factors of 1:20:120 for Cr^+:Mo^+:W^+. Not shown in Figure 8 is the fact that subsequent dehydrogenation of primary products (forming species such as MC^+ and MCH^+) is most pronounced in the tungsten system, with appreciable amounts seen for molybdenum and none for chromium.

Most of these differences in reactivity can be understood simply on the basis of differences in thermochemistry. As shown in Figure 2, the hydride and methyl BDEs of chromium, molybdenum, and tungsten cations are similar, with increases down the periodic table that reflect the lowering of the threshold for MH^+ production seen in Figure 8. In contrast, the $MoCH^+$ and $MoCH_2^+$ bonds are stronger than the chromium analogues by 2.3 and 1.3 eV, respectively, and those for WCH^+ and WCH_2^+ are stronger still by another 0.7 and 1.2 eV. Thus, formation of all products but MH^+ and MCH_3^+ are energetically more favorable in the molybdenum system by over 1 eV compared to the chromium system and enhanced for tungsten by about another 1 eV. This clearly explains the differences noted above, namely, the similarity of the MH^+ cross sections and the relative efficiencies of the initial and all subsequent dehydrogenation processes.

A more subtle difference between these three metal systems can be ascertained by noting the difference in absolute magnitudes of the MH^+ and MCH_2^+ cross sections, Figure 8. These are almost equal for molybdenum, WH^+ is somewhat smaller than WCH_2^+, and CrH^+ is much larger than $CrCH_2^+$. Our analysis of the chromium cross sections showed that formation of CrH^+ occurs primarily (~75%) by a direct abstraction process with some contributions from dissociation of a $HCrCH_3^+$ intermediate that also leads to $CrCH_2^+ + H_2$.[43] Our phase space analysis of the molybdenum cross sections indicates that approximately one-half of the MoH^+ cross section can be attributed to decomposition of a $HMoCH_3^+$ intermediate, which means that some contributions from a direct process are also occurring. In the case of tungsten, dehydrogenation is very efficient (occurring on ~20% of all collisions).[44] Because the $HWCH_3^+$ intermediate is formed so efficiently, most if not all of the WH^+ results from decomposition of this species at higher energies.

6. Conclusion

Ground-state Mo^+ ions are found to be reactive with CH_4 over a wide range of kinetic energies. Efficient dehydrogenation is observed at low energies. At high energies, the dominant process is C−H bond cleavage to form $MoH^+ + CH_3$, although there are also appreciable contributions from $MoCH_3^+$ and products that result from dehydrogenation of the primary products, MoC^+ and $MoCH^+$. The endothermic reaction cross sections observed in all three systems are modeled to yield 0 K bond dissociation energies for several Mo−ligand cations, as summarized in Table 3. Reasonable agreement is found for these values compared with theoretical work, although theory is found to underestimate the Mo^+-CH_2 and Mo^+-CH bond energies somewhat.

The mechanism for the reaction of Mo^+ with methane is discussed in some detail and elucidated using ab initio calculations of the potential-energy surfaces. This makes it evident that an initial approach on the reactant's sextet spin surface converts to the quartet spin surface upon activation of the CH bond. Modeling of the kinetic-energy dependence observed for the dehydrogenation reaction using a phase space theory approach suggests that the efficiency of this spin flip follows a Landau−Zener probability. Once the quartet $H-Mo^+-CH_3$ intermediate is formed, it can dehydrogenate via a four-centered transition state and at higher energies decomposes by simple bond fission, processes that are all spin allowed. When compared to Cr^+ and W^+, the first- and third-row transition-metal congeners, Mo^+ is found to have intermediate reactivity. This trend can be attributed largely to much stronger π bonds as one moves down the periodic table.

Acknowledgment. This research is supported by the National Science Foundation, Grant No. CHE-0451477. Dr. M. R. Sievers is thanked for collecting all the data.

Supporting Information Available: Table S1 provides theoretical energies and zero-point energies of reactants and products calculated at several levels of theory. Energies and structures of reactant and product ground and excited states calculated at the B3LYP/HW/6-311++G(3df,3p) level of theory are given in Tables S2 and S3. Theoretical energies and structures of $[Mo,C,4H]^+$ intermediates and transition states calculated at the B3LYP/HW/6-311++G(3df,3p) and B3LYP/SD/6-311++G(3df,3p) levels of theory are provided in Tables S4 and S5. This material is available free of charge via the Internet at http://pubs.acs.org.

References and Notes

(1) For reviews, see: Armentrout, P. B. In *Selective Hydrocarbon Activation: Principles and Progress*; Davies, J. A., Watson, P. L., Greenberg, A., Liebman, J. F., Eds.; VCH: New York, 1990; p 467. Armentrout, P. B. In *Gas-Phase Inorganic Chemistry*; Russell, D. H., Ed.; Plenum: New York, 1989; p 1. Armentrout, P. B.; Beauchamp, J. L. *Acc. Chem. Res.* **1989**, *22*, 315.

(2) For reviews, see: Armentrout, P. B. *Science* **1991**, *251*, 175. Armentrout, P. B. *Annu. Rev. Phys. Chem.* **1990**, *41*, 313.

(3) Weisshaar, J. C. *Adv. Chem. Phys.* **1992**, *82*, 213. Weisshaar, J. C. *Acc. Chem. Res.* **1993**, *26*, 213.

(4) van Koppen, P. A. M.; Kemper, P. R.; Bowers, M. T. *J. Am. Chem. Soc.* **1992**, *114*, 1083, 10941. van Koppen, P. A. M.; Kemper, P. R.; Bowers, M. T. In *Organometallic Ion Chemistry*; Freiser, B. S., Ed.; Kluwer: Dordrecht, 1995; pp 157−196.

(5) Allison, J. *Prog. Inorg. Chem.* **1986**, *34*, 627. Squires, R. R. *Chem. Rev.* **1987**, *87*, 623. *Gas Phase Inorganic Chemistry*; Russell, D. H., Ed.; Plenum: New York, 1989. Eller, K.; Schwarz, H. *Chem. Rev.* **1991**, *91*, 1121.

(6) Armentrout, P. B.; Georgiadis, R. *Polyhedron* **1988**, *7*, 1573.

(7) Armentrout, P. B.; Kickel, B. L. In *Organometallic Ion Chemistry*; Freiser, B. S., Ed.; Kluwer: Dordrecht, 1995; pp 1−45.

(8) *Organometallic Ion Chemistry*; Freiser, B. S., Ed.; Kluwer: Dordrecht, 1995.

(9) Armentrout, P. B. *Organometallic Bonding and Reactivity*; Brown, J. M., Hofmann, P., Eds.; Topics in Organometallic Chemistry; Springer-Verlag: Berlin, 1999; Vol. 4, pp 1−45.

(10) Crabtree, R. H. *Chem. Rev.* **1985**, *85*, 245.

(11) Schilling, J. B.; Beauchamp, J. L. *Organometallics* **1988**, *7*, 194.

(12) Blomberg, M. R. A.; Siegbahn, P. E. M.; Svensson, M. *J. Phys. Chem.* **1994**, *98*, 2062.

(13) Blomberg, M. R. A.; Siegbahn, P. E. M.; Svensson, M.; Wennerberg, J. *Energetics of Organometallic Species*; Martinho Simoes, J. A., Ed.; Kluwer: Dordrecht, 1992; pp 387−421.

(14) Cassady, C. J.; McElvany, S. W. *Organometallics* **1992**, *11*, 2367−2377.

(15) Sunderlin, L. S.; Armentrout, P. B. *J. Am. Chem. Soc.* **1989**, *111*, 3845.

(16) Armentrout, P. B.; Sievers, M. R. *J. Phys. Chem. A* **2003**, *107*, 4396.

(17) Sievers, M. R.; Chen, Y.-M.; Haynes, C. L.; Armentrout, P. B. *Int. J. Mass Spectrom.* **2000**, *195/196*, 149.

(18) Chen, Y.-M.; Armentrout, P. B. *J. Phys. Chem.* **1995**, *99*, 10775.

(19) Chen, Y.-M.; Sievers, M. R.; Armentrout, P. B. *Int. J. Mass Spectrom. Ion Processes* **1997**, *167/168*, 195.

(20) Chen, Y.-M.; Armentrout, P. B. *J. Phys. Chem.* **1995**, *99*, 11424.

(21) Sievers, M. R.; Chen, Y.-M.; Elkind, J. L.; Armentrout, P. B. *J. Phys. Chem.* **1996**, *100*, 54.

(22) Sievers, M. R.; Chen, Y.-M.; Armentrout, P. B. *J. Chem. Phys.* **1996**, *105*, 6322.

(23) Sallans, L.; Lane, K. R.; Squires, R. R.; Freiser, B. S. *J. Am. Chem. Soc.* **1985**, *107*, 4379−4385.

(24) Schilling, J. B.; Goddard, W. A., III; Beauchamp, J. L. *J. Am. Chem. Soc.* **1987**, *109*, 5565.

(25) Pettersson, L. G. M.; Bauschlicher, C. W., Jr.; Langhoff, S. R.; Partridge, H. *J. Chem. Phys.* **1987**, *87*, 481.

(26) Das, K. K.; Balasubramanian, K. *J. Chem. Phys.* **1989**, *91*, 6254.

(27) Siegbahn, P. E. M.; Blomberg, M. R. A.; Svensson, M. *Chem. Phys. Lett.* **1994**, *223*, 35.

(28) Bauschlicher, C. W., Jr.; Partridge, H.; Sheehy, J. A.; Langhoff, S. R.; Rosi, M. J. *Phys. Chem.* **1992**, *96*, 6969.

(29) Bauschlicher, C. W., Jr.; Langhoff, S. R.; Partridge, H.; Barnes, L. A. *J. Chem. Phys.* **1989**, *91*, 2399.

(30) Schilling, J. B.; Goddard, W. A.; Beauchamp, J. L. *J. Am. Chem. Soc.* **1987**, *109*, 5573.

(31) van Koppen, P. A. M.; Brodbelt-Lustig, J.; Bowers, M. T.; Dearden, D. V.; Beauchamp, J. L.; Fisher, E. R.; Armentrout, P. B. *J. Am. Chem. Soc.* **1990**, *112*, 5663. **1991**, *113*, 2359.

(32) van Koppen, P. A. M.; Bowers, M. T.; Fisher, E. R.; Armentrout, P. B. *J. Am. Chem. Soc.* **1994**, *116*, 3780.

(33) van Koppen, P. A. M.; Bowers, M. T.; Haynes, C. L.; Armentrout, P. B. *J. Am. Chem. Soc.* **1998**, *120*, 5704.

(34) Haynes, C. L.; Fisher, E. R.; Armentrout, P. B. *J. Phys. Chem.* **1996**, *100*, 18300.

(35) Noll, R. J.; Yi, S. S.; Weisshaar, J. C. *J. Phys. Chem.* **1998**, *102*, 386.

(36) Perry, J. K., Ph.D. Thesis, Caltech, 1994.

(37) Holthausen, M. C.; Fiedler, A.; Schwarz, H.; Koch, W. *J. Phys. Chem.* **1996**, *100*, 6236.

(38) Holthausen, M. C.; Koch, W. *Helv. Chim. Acta* **1996**, *79*, 1939.

(39) Holthausen, M. C.; Koch, W. *J. Am. Chem. Soc.* **1996**, *118*, 9932.

(40) Yi, S. S.; Blomberg, M. R. A.; Siegbahn, P. E. M.; Weisshaar, J. C. *J. Phys. Chem.* **1998**, *102*, 395.

(41) Freas, R. B.; Ridge, D. P. *J. Am. Chem. Soc.* **1980**, *102*, 7131. Reents, W. D.; Strobel, F.; Freas, R. B.; Wronka, J.; Ridge, D. P. *J. Phys. Chem.* **1985**, *89*, 5666.

(42) Halle, L. F.; Armentrout, P. B.; Beauchamp, J. L. *J. Am. Chem. Soc.* **1981**, *103*, 962.

(43) Georgiadis, R.; Armentrout, P. B. *J. Phys. Chem.* **1988**, *92*, 7067.

(44) Armentrout, P. B.; Shin, S.; Liyanage, R. *J. Phys. Chem A* **2006**, *110*, 1242.

(45) Ervin, K. M.; Armentrout, P. B. *J. Chem. Phys.* **1985**, *83*, 166.

(46) Schultz, R. H.; Armentrout, P. B. *Int. J. Mass Spectrom. Ion. Processes* **1991**, *107*, 29.

(47) Aristov, N.; Armentrout, P. B. *J. Am. Chem. Soc.* **1985**, *108*, 1806.

(48) Chesnavich, W. J.; Bowers, M. T. *J. Phys. Chem.* **1979**, *83*, 900.

(49) Armentrout, P. B. *Advances in Gas-Phase Ion Chemistry*; Adams, N. G., Babcock, L. M., Eds.; JAI: Greenwich, 1992; Vol. 1, pp 83−119.

(50) Shimanouchi, T. *Table of Molecular Vibrational Frequencies*; National Bureau of Standards: Washington, DC, 1972; Consolidated, Vol. I.

(51) Becke, A. D. *J. Chem. Phys.* **1993**, *98*, 5648.

(52) Lee, C.; Yang, W.; Parr, R. G. *Phys. Rev. B* **1988**, *37*, 785.

(53) Stephens, P. J.; Devlin, F. J.; Chabalowski, C. F.; Frisch, M. J. *J. Phys. Chem.* **1994**, *98*, 11623.

(54) Frisch, M. J.; Trucks, G. W.; Schlegel, H. B.; Scuseria, G. E.; Robb, M. A.; Cheeseman, J. R.; Montgomery, J. A., Jr.; Vreven, T.; Kudin, K. N.; Burant, J. C.; Millam, J. M.; Iyengar, S. S.; Tomasi, J.; Barone, V.; Mennucci, B.; Cossi, M.; Scalmani, G.; Rega, N.; Petersson, G. A.; Nakatsuji, H.; Hada, M.; Ehara, M.; Toyota, K.; Fukuda, R.; Hasegawa, J.; Ishida, M.; Nakajima, T.; Honda, Y.; Kitao, O.; Nakai, H.; Klene, M.; Li, X.; Knox, J. E.; Hratchian, H. P.; Cross, J. B.; Bakken, V.; Adamo, C.; Jaramillo, J.; Gomperts, R.; Stratmann, R. E.; Yazyev, O.; Austin, A. J.; Cammi, R.; Pomelli, C.; Ochterski, J. W.; Ayala, P. Y.; Morokuma, K.; Voth, G. A.; Salvador, P.; Dannenberg, J. J.; Zakrzewski, V. G.; Dapprich, S.; Daniels, A. D.; Strain, M. C.; Farkas, O.; Malick, D. K.; Rabuck, A. D.; Raghavachari, K.; Foresman, J. B.; Ortiz, J. V.; Cui, Q.; Baboul, A. G.; Clifford, S.; Cioslowski, J.; Stefanov, B. B.; Liu, G.; Liashenko, A.; Piskorz, P.; Komaromi, I.; Martin, R. L.; Fox, D. J.; Keith, T.; Al-Laham, M. A.; Peng, C. Y.; Nanayakkara, A.; Challacombe, M.; Gill, P. M. W.; Johnson, B.; Chen, W.; Wong, M. W.; Gonzalez, C.; Pople, J. A. *Gaussian 03*, Revision B.02; Gaussian, Inc.: Wallingford CT, 2004.

(55) Foresman, J. B.; Frisch, Æ. *Exploring Chemistry with Electronic Structure Methods*, 2nd ed.; Gaussian: Pittsburgh, 1996.

(56) Hay, P. J.; Wadt, W. R. *J. Chem. Phys.* **1995**, *82*, 299.

(57) The basis sets used for Mo were obtained from the Extensible Computational Chemistry Environment Basis Set Database, version 10/29/02, as developed and distributed by the Molecular Science Computing Facility, Environmental and Molecular Sciences Laboratory which is part of the Pacific Northwest Laboratory, P.O. Box 999, Richland, WA 99352 and funded by the U.S. Department of Energy. The Pacific Northwest Laboratory is a multiprogram laboratory operated by Battelle Memorial Institute for the U.S. Department of Energy under contract DE-AC06−76RLO 1830.

(58) Andrae, D.; Haeussermann, U.; Dolg, M.; Stoll, H.; Preuss H. *Theor. Chim. Acta* **1990**, *77*, 123.

(59) Ehlers, A. W.; Böhme, M.; Dapprich, S.; Boggi, A.; Höllwarth, A.; Jonas, V.; Köhler, K. F.; Stegmann, R.; Veldkamp, A.; Frenking, G. *Chem. Phys. Lett.* **1993**, *208*, 111.

(60) Holthausen, M. C.; Heinemann, C.; Cornehl, H. H.; Koch, W.; Schwarz, H. *J. Chem. Phys.* **1995**, *102*, 4931.

(61) Holthausen, M. C.; Mohr, M.; Koch, W. *Chem. Phys. Lett.* **1995**, *240*, 245.

(62) Møller, C.; Plesset, M. S. *Phys. Rev.* **1934**, *46*, 618.

(63) Pople, J. A.; Head-Gordon, M.; Raghavachari, K. *J. Chem. Phys.* **1987**, *87*, 5968.

(64) Moore, C. E. *Atomic Energy Levels, NSRDS−NBS* **1971**, *35, Vol. III*, 1.

(65) Armentrout, P. B. Work in progress.

(66) Aristov, N.; Armentrout, P. B. *J. Am. Chem. Soc.* **1984**, *106*, 4065.

(67) Elkind, J. L.; Armentrout, P. B. *J. Phys. Chem.* **1987**, *86*, 1868.

(68) Fisher, E. R.; Armentrout, P. B. *J. Am. Chem. Soc.* **1992**, *114*, 2039.

(69) Georgiadis, R.; Armentrout, P. B. *Int. J. Mass Spectrom. Ion Processes* **1989**, *89*, 227.

(70) Zhang, X.-G.; Rue, C.; Shin, S.-Y.; Armentrout, P. B. *J. Chem. Phys.* **2002**, *116*, 5574.

(71) Irikura, K. K.; Beauchamp, J. L. *J. Phys. Chem.* **1991**, *95*, 8344.

(72) Ohanessian, G.; Goddard, W. A. , III *Acc. Chem. Res.* **1990**, *23*, 386.

(73) Zhang, X.-G.; Liyanage, R.; Armentrout, P. B. *J. Am. Chem. Soc.* **2001**, *123*, 5563.

(74) Armentrout, M. M.; Li, F.-X.; Armentrout, P. B. *J. Phys. Chem. A* **2004**, *108*, 9660.

(75) Clemmer, D. E.; Aristov, N.; Armentrout, P. B. *J. Phys. Chem.* **1993**, *97*, 544.

(76) Gioumousis, G.; Stevenson, D. P. *J. Chem. Phys.* **1958**, *29*, 294.

(77) Rue, C.; Armentrout, P. B.; Kretzschmar, I.; Schröder, D.; Harvey, J. N.; Schwarz, H. *J. Chem. Phys.* **1999**, *110*, 7858.

(78) Landau, L. D. *Phys. Z. Sowjetunion* **1932**, *2*, 46. Zener, C. *Proc. R. Soc. London Ser. A* **1932**, *137*, 696. Stueckelberg, E. C. G. *Helv. Phys. Acta* **1932**, *5*, 369.

(79) Baer, T.; Hase, W. L. *Unimolecular Reaction Dynamics*; Oxford: New York, 1996; p 316 and references therein.

(80) Heller, E. J.; Brown, R. C. *J. Chem. Phys.* **1983**, *79*, 3336.

(81) Lorquet, J. C.; Leyh-Nihant, B. *J. Phys. Chem.* **1988**, *92*, 4778.

(82) Aristov, N.; Armentrout, P. B. *J. Phys. Chem.* **1987**, *91*, 6178.